Results in Physics 18 (2020) 103281

Contents lists available at ScienceDirect

Results in Physics

journal homepage: www.elsevier.com/locate/rinp

Numerical development of high performance quasi D-shape PCF-SPR biosensor: An external sensing approach employing gold

Md. Biplob Hossain[a,1,2], Md Shafayet Hossain[b,1], S.M. Riazul Islam[c,1], Md. Nazmus Sakib[d], Khondoker Ziaul Islam[b], Md. Amzad Hossain[a], Md. Sanwar Hossain[b], A.S.M. Sanwar Hosen[e], Gi Hwan Cho[e,2]

[a] Department of Electrical and Electronic Engineering, Jashore University of Science and Technology, Jashore 7408, Bangladesh
[b] Department of Electrical and Electronic Engineering, Bangladesh University of Business and Technology, Dhaka 1216, Bangladesh
[c] Department of Computer Science and Engineering, Sejong University, 209 Neungdong-ro, Gwangjin-gu, Seoul 05006, South Korea
[d] Department Electronics & Telecommunication Engineering, Rajshahi University of Engineering & Technology, Rajshahi 6204, Bangladesh
[e] Division of Computer Science and Engineering, Jeonbuk National University, Jeonju 54896, South Korea

ARTICLE INFO

Keywords:
Amplitude sensitivity
Wavelength sensitivity
SPR
Resolution
Dual core-PCF

ABSTRACT

In this paper, a proper concept of a kind of photonic crystal fiber known as D-shaped PCF sensor based on SPR or Surface Plasmon Resonance phenomenon has been discussed. The analysis has been performed numerically using FEM or Finite Element Method and PML (Perfectly Matched Layer) boundary conditions. Modal analysis has been performed keeping the smallest mesh as possible. The main mechanism of the sensor is the interaction between the core guided light beam and the metal layer surface that generates free electrons. The proposed sensor shows a refractive index detection range of 1.42–1.46 RIU, with a metal thickness variation of 35 nm-45 nm and a pitch variation of 1.8 μm–2.0 μm. The sensor obtained the highest sensitivity of 15000 nm/RIU with a maximum 6.67 × 10^{-6} RIU resolution, using the wavelength interrogation method. Average spectral sensitivity is 8000 nm/RIU. The amplitude interrogation method found a maximum sensitivity of 230 RIU^{-1} with a resolution of 4.348 × 10^{-5} RIU. The sensor also shows high linearity fitting and Figure of Merit (FoM). For ease of design, high detection range, high wavelength and amplitude sensitivity, less fabrication complexity, high linearity and stability, the sensor can be a great competitor of the PCF sensors previously proposed.

Introduction

In this recent era, the SPR biosensors have been dominating the reign of biomedical engineering. The SPR biosensors have been widely used to detect unknown analytes to diagnostic diseases, measure the density of proteins and fibrinogens, detect coagulation, antigens and antibodies, and identify the toxin, environment safety, temperature sensing etc.

The term SPR (Surface Plasmon Resonance) defines a phenomenon that occurs due to the interface of nano-level metal layer and pole polarized lights evanescent from the core when light beams are incident from the core to metal surfaces and reduces free electrons. When the wavelength of core mode light particles and the plasmon mode coincide with each other, there is a huge transmission loss of energy from the core to the metal surface and eventually the resonance occurs. This wavelength is called resonance wavelength. The intersecting point of the real part of the core mode and plasmon mode loss graph indicates the resonant wavelength [34].

The idea of SPR phenomenon came in the early 20th century, from the diffraction of light intensity on wood [35]. SPR was first found theoretically by Ritchie *et al.* in the 1950s [36]. Kretschmann proposed a configuration of SPR sensor based on prism coupling [37]. In that configuration, a light beam is incident on one plane of the prism as a transverse wave, which becomes pole-polarized and reflects on the metal surface which is placed on the other facet. Since then prism coupling SPR sensors have been used worldwide. But due to the bulky configuration, heavy weight, inflexibility, inability of remote sensing, and construction complexity- this sensor could not last long, when the configuration of PCF sensor arrived [37]. PCF means Photonic Crystal Fiber which is made of core of fiber optics and periodically arranged air holes around the core which forms the cladding [38]. The PCF based sensor was first introduced by R.C. Jorgenson, where a thin metal layer

E-mail address: biplobh.eee10@gmail.com (Md. Biplob Hossain).
[1] These authors contributed equally to this work and co-first authors.
[2] These authors are co-corresponding authors.

https://doi.org/10.1016/j.rinp.2020.103281
Received 30 April 2020; Received in revised form 19 June 2020; Accepted 29 July 2020
Available online 02 August 2020

of gold was used to create the SPR phenomenon [38]. From then the era of prism coupling has ended and the new era is still leading because of its high sensitivity, high confinement loss, less fabrication complexity, high detection range and good remote sensing. But still there remains a limitation in phase matching of the metal free electron and the incident p-polarized light on the surface [34].

To date, different SPR sensor structures have been introduced, such as internal coating, external coating, and, circular-shape [39–44]. Among them, external coating PCF based SPR sensor is highly studied due to its ease of fabrication. Hasan *et al* in [20], have proposed a spiral PCF sensor for an external bio-sensing approach. It shows an amplitude sensitivity of 371.5 RIU^{-1} and a wavelength sensitivity of 4600 nm/RIU for *x*-polarized direction. Therefore, the sensitivity is acceptable but not preferable on the perspective of updating technology. Very recently, Singh *et al.* in [21], proposed a titanium nitride (TiN) coated PCF-SPR sensor for external bio-samples detection, which shows a better wavelength sensitivity of 10,000 nm/RIU [21]. However, this sensor shows a very narrow samples detection range. In October 2018, Jiao *et al.* proposed a sliver nano-continuous grating sensor with wavelength sensitivity of 13,600 nm/RIU [45]. But it was too complex to fabricate this type of configuration. Ahmed *et al.* in November 2019, proposed a hexagonal lattice fiber sensor with sensitivity of 16,000 nm/RIU with detection range 1.33 to 1.40 [46]. But in this configuration we need more metal coating and much analyte to detect around the whole fiber.

In the proposed sensor we tried to achieve maximum sensitivity. To complete the core, we used fused silica for its very weak temperature sensitivity [6–12]. And a gold film for its chemical stability and larger resonance wavelength shift. The proposed sensor is analyzed and simulated numerically using the Finite Element Method with a smaller mesh analysis. To prevent light from dispersing out of the fiber, PML boundary condition was applied. In a conventional PCF sensor there is a difficulty in placement of metal thin film. To avoid this difficulty, we polished one side of the surface to make a small plane surface and put the thin film on the flat plane filling its top with analyte. To form its cladding, three air hole rings were made using laser appliance.

In Quasi D-shape structure, sample can flow throughout the outer surface of the structure. Hence the sensor structure becomes simpler. The proposed D-sensor requires less polishing complexity and is easy to place metal thin film and change the analyte frequently for detection and less fabrication cost. Our proposed sensor shows higher sensitivity, a high figure of merit, high linearity and resolution, high detection range and low manufacturing cost. We have analyzed our sensor by varying the thickness of the metal film, the refracting index of the analyte, the pitch and air hole diameter to check its sensing performance and by finding its highest sensitivity and detection range.

Design and theoretical background

The 2-D cross section view representation of the offered biosensor is shown in Fig. 1.

The PCF lattice is formed with three air hole formed rings with one missing hole in the second circular ring. The one missing air-hole in the second circular ring is used to create birefringence and four air-holes in the third ring are made relatively small to produce an evanescent field and therefore surface plasmon can be excited easily.

In this structure, the air-hole's center-center distance is called pitch (Λ), the diameter of the small air-hole is indicated by d_s and the large air-hole diameter is denoted by d_1. Here, Λ = 1.9 μm, d_s = 0.25Λ and d_1 = 0.5Λ. The diameter of the PCF is 9.5 μm. The gold layer having a variable thickness (t_s) is coated on the outer region of the PCF fiber using chemical vapor deposition method (CVD) which performs as the noble and active plasmonic metals for the proposed device. The fused silica is used as fiber background material. To characterize the refractive index complex part (RI) of fused silica, the Sellmier equation is used, which is defined as [14–17,22]:

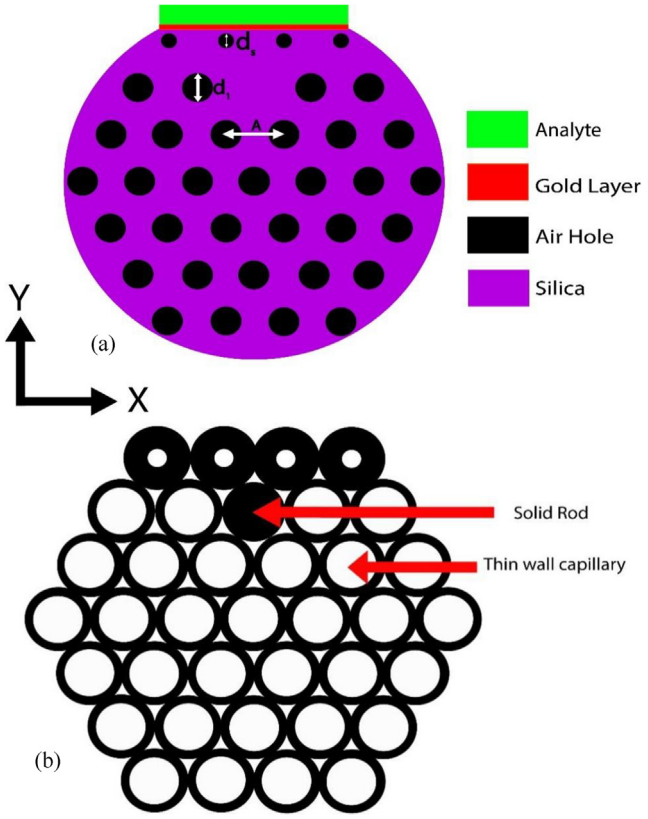

Fig. 1. (a) Cross section view and (b) Stacked view of the expressed quasi D-shaped lattice PCF-SPR sensor with Λ = 1.9 μm, *ds* = 0.25Λ, d_1 = 0.5Λ and t_g = 40 nm.

$$n^2(\lambda) = 1 + \frac{B_1\lambda^2}{\lambda^2 - C_1} + \frac{B_2\lambda^2}{\lambda^2 - C_2} + \frac{B_3\lambda^2}{\lambda^2 - C_3} \quad (1)$$

where n is the RI of fused silica which is a wavelength dependent expressed in μm. The B_1, B_2, B_3, C_1, C_2, C_3 are the Sellmeier constant given in literature [19]. Here B_1 = 0.69616300, B_2 = 0.407942600, B_3 = 0.897479400, C_1 = 0.00467914826, C_2 = 0.0135120631, C_3 = 97.9340025. The constants of the above equation were taken from the Ref [19].

The gold's dielectric constant can be obtained by the Drude-Lorentz model formula which is given by [31],

$$\varepsilon_{Au} = \varepsilon_\infty - \frac{\omega_D^2}{\omega(\omega + j\gamma_D)} - \frac{\Delta\varepsilon\cdot\Omega_L^2}{(\omega^2 - \Omega_L^2) + j\Gamma_L\omega} \quad (2)$$

where ε_{Au} denotes gold permittivity; the high frequency permittivity is identified by ε_m, the frequency of plasma is ωD, the angular frequency is ω, and the damping frequency is ϒD. Here ε_∞ = 5.9673, ω = 2πc/λ. Here, c denotes the light velocity in the vacuum, ωD/2π = 2113.6 THz, ϒD/2π = 15.92 THz and the weighting factor is Δε = 1.09. Moreover, Lorentz spectral width ΓL/2π = 104.86 THz and the strength of the oscillator is ΩL/2π = 650.07 THz. The sensing layer is deposited on the outer portion of the gold thin film layer to detect the targeted molecules efficiently.

Results analysis and discussion

The numerical analysis of the proposed dual core-Quasi D shape photonic crystal fiber-based plasmonic RI Sensor has been accomplished by the FEM based COMSOL software. The sensing layer is deposited on the outer portion of the gold thin film layer to detect the targeted molecules efficiently. A constant liquid layer of thickness 1.5 μm was used for simulation. We kept the mesh element size of as

small as possible to us so that we can easily map smaller air-holes. The circular perfectly matched layer or PML is also placed on the upper portion of the analyte as a boundary condition. The finer meshing elements used here during simulation to map the smaller air-hole correctly. Total 18,359 triangular elements used here to represent the meshed computational domain of the sensor where edge elements are of 1722 and vertex elements are of 103 along total mesh area is of 507.8 μm^2.

The working mechanism of the PCF-SPR sensor depends on the combined interaction of the momentary field and the surface free electron of the dielectric metal surface. Light that propagates in the fiber core generates an evanescent field in the cladding. At the particular wavelength effective refractive index (n_{eff}) a real part of the core and surface plasmon polariton (SPP) mode coincide. Due to interaction of the core-clad evanescent field, an electron is emitted from the metal surface. As a result, a surface plasmon wave is generated. The numerical analysis of the proposed plasmonic sensor is discussed by observing the confinement loss of the sensor which is the function of different analyte RIs' wavelength, can be characterized by using the following formula [20,23]:

$$\alpha(dB/cm) = 8.686 \times k_o \,\mathrm{Im}(n_{eff}) \times 10^4 \tag{3}$$

where $k_o = \frac{2\pi}{\lambda}$ is a number of wave and Im(n_{eff}) is the effective imaginary mode index. During the

simulation, we performed only *y*-polarized mode because of the improved effective mode index and higher radiation loss observed in that direction compared to the *x*-polarized mode. The dispersion relation with EM field distribution is illustrated in Fig. 2. Mathematically, resonance occurs when the (confinement loss) effective mode real and imaginary index of the SPP mode and the core modes are identical. The modal analysis is performed on an *xy*-plane while the wave is propagated in the direction of z. The offered fiber indicates birefringence because of the plasmonic structure. The *y*-polarization has a greater electric field near the surface of the metal, thus, the momentary field can easily interact with the gold film layer paralleled to the fundamental *x*-polarized light. So we consider the *y* component as fundamental mode. The sensor electric field and phase matching property are given in Fig. 2(a), 2(b) and 2(c). From Fig. 2(d), it is evident that resonance occurred at wavelength 1.3 μm for an analyte RI of 1.43 RIU. This is the point of phase matching, and at that resonance point, a sharp loss peak is obtained which means the highest energy can be propagated from the fundamental mode to the plasmonic mode along the *x*-polarized direction.

Wavelength sensitivity and corresponding resolution

Wavelength sensitivity is a crucially important parameter for performance calculation which is defined by using wavelength interrogation technique as [1,20,23]:

$$S\lambda(nm/RIU) = \Delta\lambda peak/\Delta na \tag{4}$$

where $\Delta\lambda_{\text{peak}}$ means the wavelength variation of peaks, and Δn_{a} means the two adjacent RI variation. The curve of the loss (confinement) variation for the core guided effective mode index is depicted in Fig. 3 (a) with RI, n_a from 1.42 RIU to 1.46 RIU. The resonance or loss peaks are gradually shifted to the higher wavelengths from 1.08 μm to 1.26 μm, 1.14 μm to 1.44 μm and 1.12 μm to 1.5 μm to the n_a variation from 1.42 RIU to 1.43 RIU, 1.43 RIU to 1.44 RIU and 1.44 RIU to 1.45 RIU, respectively. The loss peaks are obtained 42 dB/cm and 112 dB/cm with an analyte RI of 1.42 RIU and 1.46 RIU respectively. Besides, the changing characteristics of the resonance wavelengths for variation of the RI are established as [24,25]:

$$n_a = n_c + c_a \frac{dn}{dc} \tag{5}$$

Here c_a is the target analyte's molecular concentration, n_c indicates the RI of probe analyte only (no target analyte) and $\frac{dn}{dc}$ is increase rate in RI due to adsorbate immobilization. The considered rate of increasing parameter value$\frac{dn}{dc}$=0.182 cm^3/gm as in standard cases [2,3,25] while using water. As a discerning dielectric RI changes with the adscription of target analyte particles, SPR wavelength shifts in right. Biomolecular analyte as electron-affluent molecule changes the carrier's concentration in dielectric-metal (Au, here) alliance which causes the variation of propagation constant. If a change in wave vector (propagation constant), the resonance wavelength of SPW is also changed which is explained in the literature mathematically [4,5,25] as given below:

$$\lambda_{peak} = \frac{2\Pi}{K_{SPW}} n_a \sin\theta_{in} \tag{6}$$

where, θ_{in} denotes optical light incident angle. Since the change of concentration of analyte, the RI of the analyte is also changed according to Eq. (5). Eq. (6). states that SPR wavelength changes if n_a changes which finally causes k_{spw} to change. At the point where the SP propagation constant and incident wave propagation constant are identical to each other, there the loss peaks are detected.

It is observed from Fig. 3, the proposed fiber has a difference between shift in peak wavelength, $\Delta\lambda_{\text{peak}}$ of 150 nm, 70 nm, 40 nm, 30 nm for RI variation Δn_{a} of 0.01, where changes in analyte RIs are 1.42 RIU to 1.43 RIU, 1.43 RIU to 1.44 RIU, 1.44 RIU to 1.45, 1.45 RIU to 1.46 RIU. Therefore, the wavelength sensitivities are computed 15000 nm/RIU, 7000 nm/RIU, 7000 and 3000 nm/RIU respectively. Average spectral sensitivity calculated is 8000 nm/RIU and 15,000 nm/RIU is the maximum sensitivity of wavelength which is as good as with previously proposed results in literature [26,27].

The sensor resolution of RI sensor is the lowest change of quantity it measures that can be detected by the sensor [22]. The resolution of sensor calculation is also imperative to quantify the detection capability of the proposed sensor, which is defined by the below equation [19]:

$$R(RIU) = \Delta n_a \times \Delta\lambda_{min}/\Delta\lambda peak \tag{7}$$

where Δn_{a} = 0.01 RIU with $\Delta\lambda_{\text{min}}$ = 0.1 nm, and considering $\Delta\lambda_{\text{peak}}$ = 150 nm. The highest resolution of the offered sensor is obtained at 6.67 × 10^{-6} RIU. As a result, the offered sensor potentially detects the 10^{-6} order's analyte RIs variation.

Amplitude sensitivity and corresponding resolation

Amplitude sensitivity is a commonly used performance parameter which defined by following equation using amplitude interrogation [20]:

$$S_A(RIU^{-1}) = -\frac{1}{\alpha(\lambda n_a)} \times \frac{\partial(\lambda, n_a)}{\partial n_a} \tag{8}$$

where $\alpha(\lambda, \eta_a)$ refers to the radiation loss and $\partial(\lambda, \eta_a)$ denotes the variation in confinement loss. Sensitivity of amplitude with analyte RI (n_{a}) variation from 1.46 RIU to 1.48 RIU is revealed in Fig. 3 (b). Using equation (8), the sensitivities are obtained 300 RIU^{-1}, 310 RIU^{-1} and 560 RIU^{-1} using optimized sensor parameters with an n_{a} of 1.46 RIU, 1.47 RIU and 1.48 RIU, respectively. Also, assuming 1% transmitted intensity, by using (7) the maximum resolution of this device is found 1.78 × 10^{-5} RIU.

Basically, the high sensitivity of the proposed sensor is owing to the enriched free electrons in the momentary field. In SP occurrence, the chief issue is to stimulate the metal surface free electrons proficiently and effectually [28,29]. In this structure, D shaped (dual core) is used which confirms that the momentary field propagates lesser equi-semi-distance to stimulate the surface electrons of the gold and it exponentially decayed as a function of distance [29]. The another factor on which the sensitivity is dependent is the strength of the SP wave. The momentary field will face longer distance and have a tendency to die out beforehand arriving at the gold metal surface because of the single core, and as a result, proficient stimulation of the free electrons will not

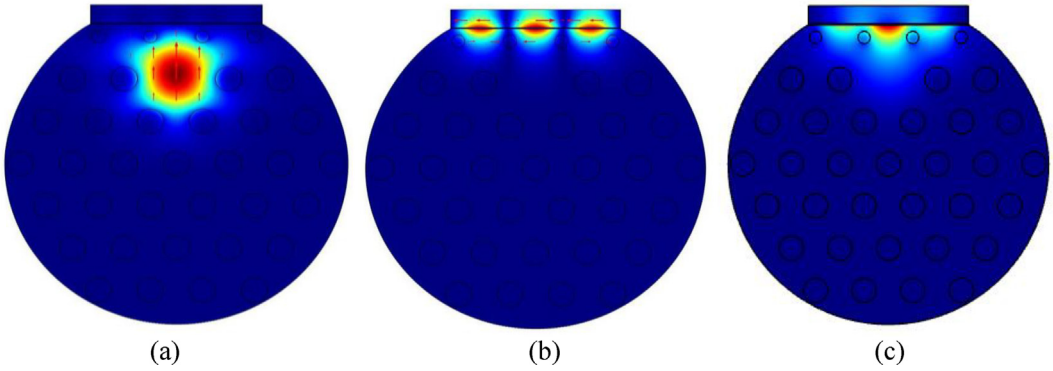

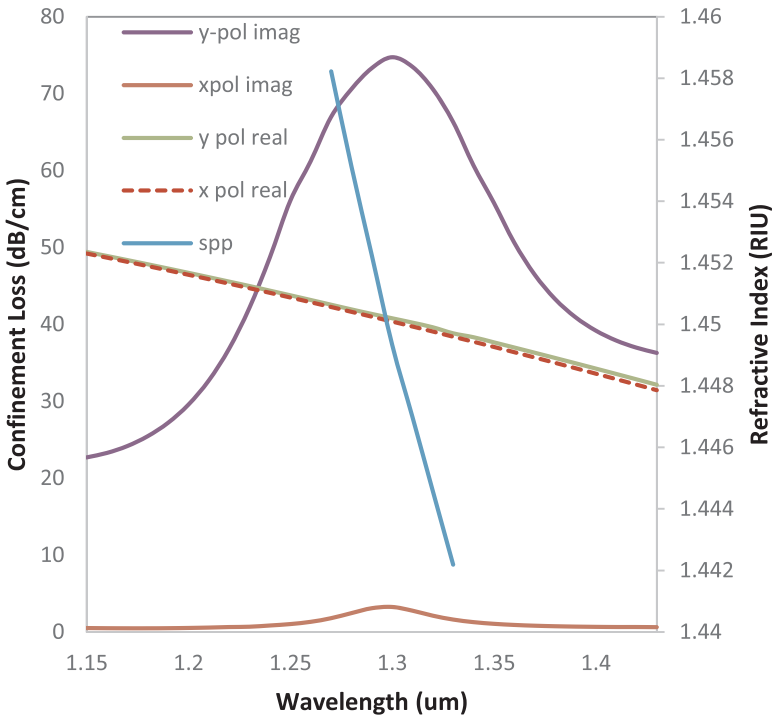

(d)

Fig. 2. Optical field distribution of (a)fundamental y-polarization core mode at 1.37 μm, (b) y-polarization SPP mode at 1.37 μm, (c) coupling mode at 1.41 μm and (d) The fundamental SPP mode and core-guided mode dispersion relation $n_a = 1.43$ and $t_g = 40$ nm.

be possible. The design technology of the proposed sensor helps the momentary field to penetrate easily into the cladding and to interact easily with the metal free electrons. These free electrons resonate when resonance occurs and due to this, SPW generation is occasioned. Correspondingly, the size of the air-holes is kept smaller than other air holes, so the momentary field comes to be an easy pathway to oscillate the gold metal surface, which increases the strength of the SP wave and improves the sensitivity.

Effect of gold layer thickness on sensitivity

Gold film layer thickness (t_s) is a crucial influence on sensing performance. The resonance wavelength can shift because of the variation of t_s. Therefore, optimization of t_s is important. Because of the excellent optical characteristics of gold (Au), the loss band and amplitude sensitivity both are reduced with the increasing as explained in Fig. 4 (a) and 4(b).

The loss peaks are shifted to a higher wavelength (right shift) and gradually decreased. With an n_a of 1.43, the loss depths are obtained 68 dB/cm, 75 dB/cm and 95 dB/cm and for analyte RI of 1.48 RIU the loss resonance peaks are achieved about 96 dB/cm, 97 dB/cm, and 98 dB/cm having the gold thin film layer thickness of 35 nm, 40 nm, and 45 nm, respectively. Besides, the amplitude sensitivities are obtained to about 200 RIU^{-1}, 125 RIU^{-1}, and 70 RIU^{-1} having the gold layer thickness of 35 nm, 40 nm, and 45 nm, respectively. From Fig. 4, t the loss of depth and sensitivity of the amplitude both have been severely reduced with the increasing of gold layer thickness. The highest sensitivity is gained at $t_s = 35$ nm.

Effect of pitch parameter on sensitivity

The center-center distance of the air hole (s) or pitch (Λ) parameter also has a vital impact on sensing response. The changes of Λ from the optimum value will be the causes the variation in loss depth and sensitivity of amplitude.

If the loss depth goes to a higher wavelength from an optimum loss,

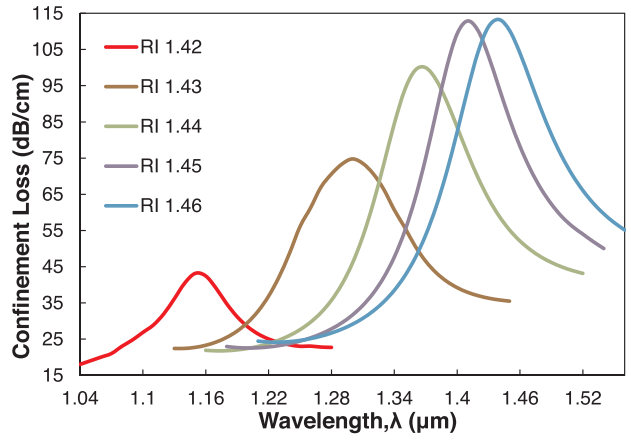

(a)

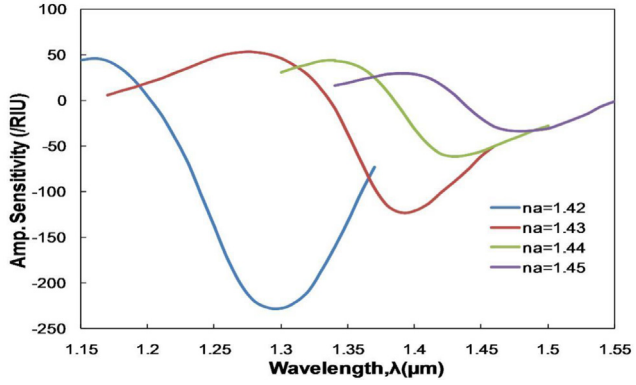

(b)

Fig. 3. (a) Fundamental loss variation for increment in analyte RI from 1.43 to 1.46 and (b) sensitivity of amplitude for different analyte RI with $\Lambda = 1.9$ μm, $d_s = 0.25\Lambda$, $d_1 = 0.5\Lambda$, and $tg = 40$ nm.

then it is called a "red shift" and if it goes to a lower wavelength it is then called a "blue shift". The change of confinement loss spectrum and amplitude sensitivity spectrum from the optimum results is shown in Fig. 5 (a) and 5(b) due to the variation of the pitch parameter. Due to the increment of the pitch from the optimum value, the loss depth is blue shifted. From Fig. 5 (a) it is seen that when the pitch parameter increases from 1.8 μm to 1.9 μm, then the loss peaks decrease from 90 dB/cm to 75 dB/cm and 120 dB/cm to 100 dB/cm for n_a of 1.43 RIU and 1.44 RIU, respectively. Besides, owing to the increment of the pitch parameter from the optimum value, the loss depth is red shifted. By enhancing, Λ from 1.9 μm to 2 μm, the corresponding loss depth is shifted from 75 dB/cm to 60 dB/cm and from 100 dB/cm to 90 dB/cm for n_a of 1.43 RIU and 1.44 RIU, respectively. Also, the amplitude sensitivities are lessened from 400 RIU^{-1} to 340 RIU^{-1} for $\Lambda = 1.9$ μm to 2 μm, respectively.

Effect of tolerance test on sensitivity

We also changed the thickness of the gold (Au) layer t_g and pitch as ± 2% and ± 5% and calculated their corresponding sensitivity for analyte RI of 1.43. We notice that for variation of the gold layer thickness, little change occurs in amplitude sensitivity and for variation of pitch, sensitivity change is negligible but a little peak shift of resonant wavelength occurs. Fig. 6(a) and 6(b) show this.

Effect of air hole diameter on sensitivity

The variation of small air-holes and large air-holes has also effected the loss spectra. We changed the value of small air-holes as 0.20Λ, 0.25Λ, 0.30Λ and obtained their corresponding amplitude sensitivity 150, 123 and 130 RIU^{-1}. If we decrease the size of air-holes, then spectral loss increases and peak shifting occurs towards the right and vice-versa. Similarly we varied the value of large air-holes as 0.45Λ, 0.50Λ, 0.55Λ and obtained their corresponding amplitude sensitivity 130, 110 and 114 RIU^{-1}. In this case, with an increase of air-hole sizes, spectral loss also increases and peak shifts towards right and vice-versa. All these are shown in Fig. 7(a), 7(b), 7(c) and 7(d).

Linear curve fitting characteristic of the resonance wavelength

The performance of the sensor can be designated with the slope of the polynomial fitting curve. Fig. 8 illustrates the polynomial fitting curve with the increase of analyte RI from 1.42 RIU to 1.46 RIU. The progressive equation for linear curve fitting can be written as y = 6.9X-8.916, where y means the resonance wavelength and × means the analyte RI. The designed D shaped air holes can be physically realized

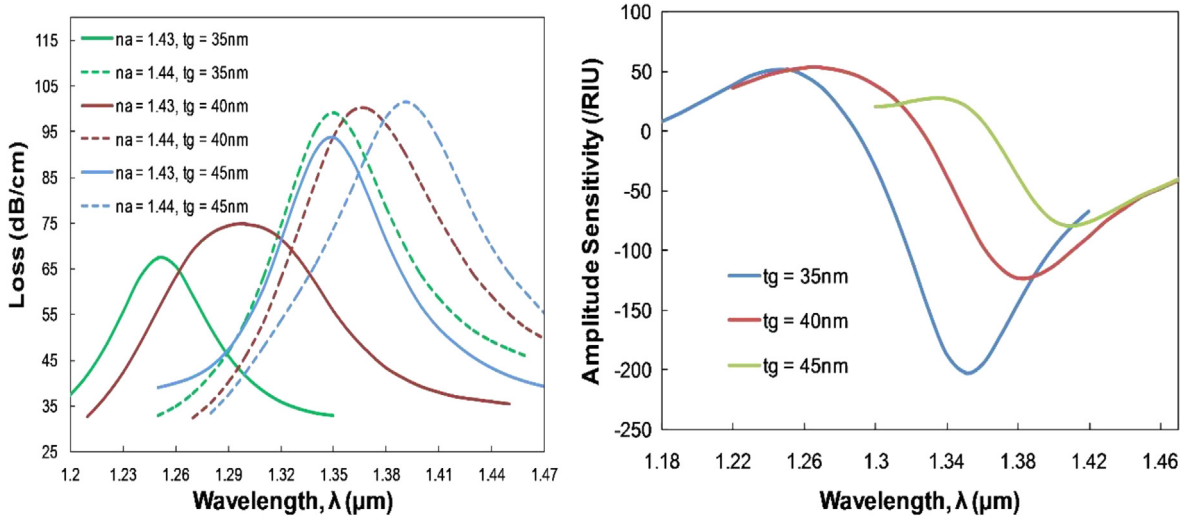

(a) (b)

Fig. 4. (a) Variation in fundamental loss of the proposed sensor for different gold film layer thicknesses and (b) Sensitivity of amplitude for different gold layer thicknesses with $\Lambda = 1.9$ μm, $d_s = 0.25\Lambda$, and $d_1 = 0.5\Lambda$ for an analyte RI of 1.43.

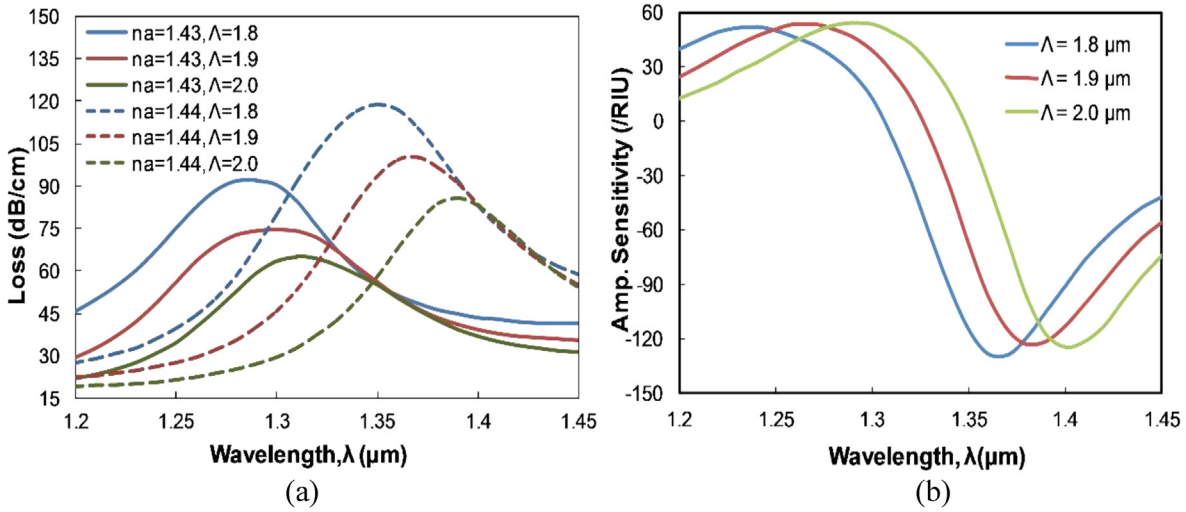

Fig. 5. (a) Fundamental loss spectrum for increase in pitch values from 1.8 to 2.0 μm; (b) sensitivity of amplitude for different pitch values with an analyte RI of 1.43.

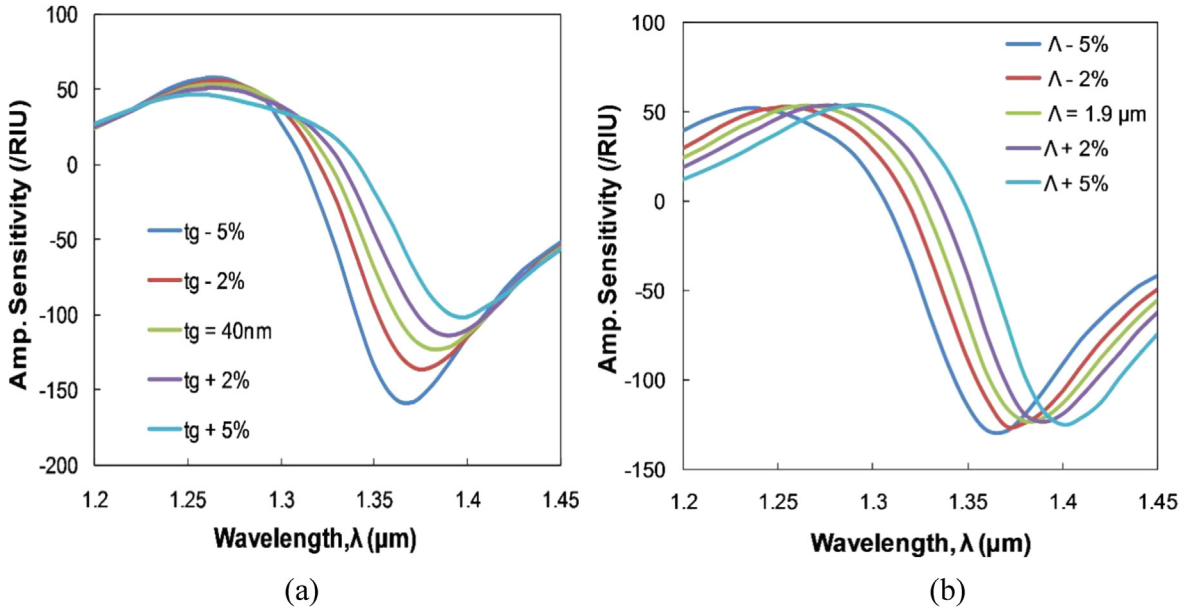

Fig. 6. (a) Sensitivity curve of ± 2% and ± 5% variation for gold layer thickness, t_g; (b) Sensitivity curve of ± 2% and ± 5% variation for pitch.

with a well-known stack-and-draw fabrication procedure. The slope of the polynomial fitting curve of the SPR wavelength has played a most important effect on average resolution and sensitivity. However, the association between the SPR wavelength and the analyte RI is nonlinear as shown in equation (6), the characteristic of polynomial fitting is very significant for the optimization of the sensor structure for getting a definite performance. The high linearity of the sensor is a requirement for the effective calibration of the sensor and denotes a good sensor especially for high RI analytes [20]. Additionally, the slope of the polynomial curve fitting signifies the average sensitivity of a sensor. The high linearity slope specifies that the sensor has a high average sensitivity and sensor resolution which makes the sensor measurement correct. Fundamentally, the nonlinear polynomial characteristic lessens the average sensitivity and resolution. A nonlinear response is not desirable, as it forms a substantial discrepancy of the average sensitivity and sensor resolution [20,22]. From Fig. 6, the measured coefficient (R^2) (here the R^2 value is obtained about 0.9972 of the proposed sensor is for x-polarization modes) shows a high linearity and ensures high average sensitivity and resolution as well.

Figure of merit (FoM)

The other factor on which the sensor performance depends is the figure of merit. A figure of merit is sometimes called a ration of signal to noise (SNR). For better design, the SNR is an important parameter. We know that the higher SNR can lead to a considerably reduced standard deviation to the variation of the spectra. Furthermore, the enhancement of SNR and spectral width will satisfy a better sensing limit for the sensor, which can be formed by using the figure of merit or FoM. The FoM is defined by [30] as:

$$FOM = \frac{S(nm/RIU)}{FWHM(nm)} \tag{9}$$

where, S denotes the linear slope of the SP wavelength depending on the RI and FWHM means the Full Width at Half-Maxima. In this analysis, the FoM of the designed fiber sensor with a gold coating layer is graphically shown in Fig. 9.

The curve of the FoM variation for the core guided effective mode index is depicted in Fig. 9 with RI, n_a from 1.42 RIU to 1.46 RIU. The FoM is gradually shifted to higher values from 30 RIU^{-1} to 45 RIU^{1}

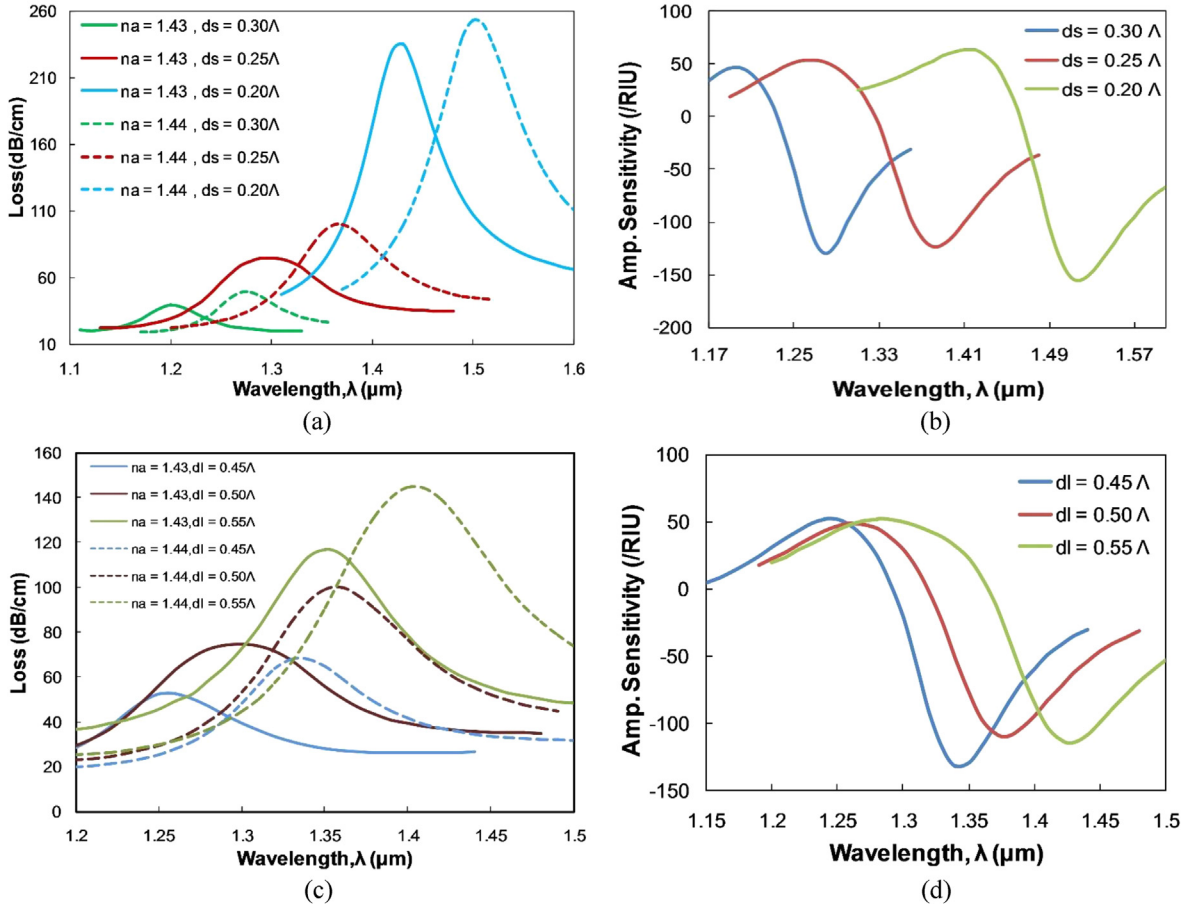

Fig. 7. (a) Fundamental loss spectrum for variation of small air-holes values 0.20Λ, 0.25Λ and 0.30Λ; (b) sensitivity of amplitude for different small air-holes values with an analyte RI of 1.43;(c) Fundamental loss spectrum for variation of large air-holes values 0.45Λ, 0.50Λ and 0.55Λ; (d) amplitude sensitivity for different large air-holes values with an analyte RI of 1.43.

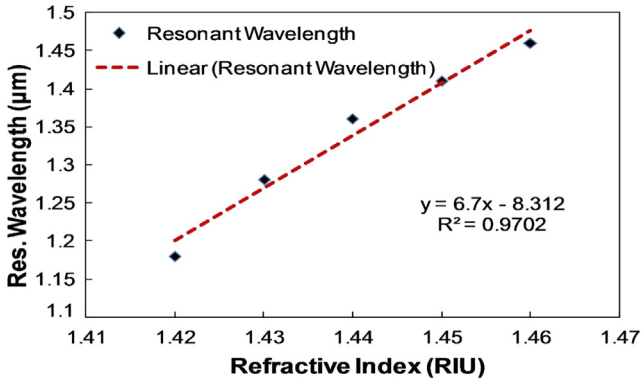

Fig. 8. Linear curve fitting of the resonance wavelength as a function of RI of analyte for $\Lambda = 1.9$ μm, $d_s = 0.25\Lambda$, $d_l = 0.5\Lambda$, and $tg = 40$ nm.

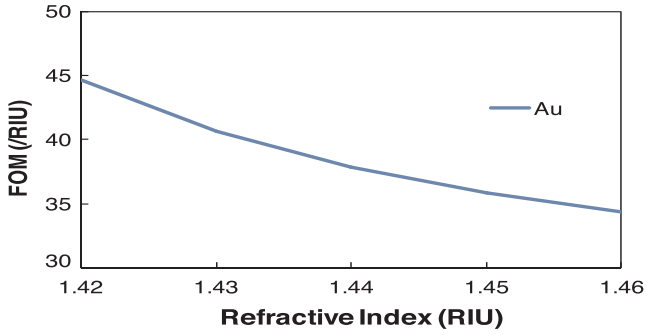

Fig. 9. Variation of the FoM with respect to analyte RI for the offered DD-PCF SPR sensor.

with respect to the n_a variation from 1.42 RIU to 1.46 RIU, respectively. The FoM is obtained by taking optimum sensor parameters with $\Lambda = 1.9$ μm, $d = d_c = 0.25\ \Lambda$, $d_l = 0.5\ \Lambda$, and $t_s = 30$ nm.

Comparative study

Lastly, we have arranged information in a tabular form that shows a comparative study among different performances of the raised SPR sensor with other existing sensors from the literature [31], [13], [32], [18] and [33] which are referred to in Table 1.

The establishment of Table 1, was made by considering the amplitude sensitivity, wavelength sensitivity, amplitude resolution and wavelength resolution. In Table 1, it is revealed that our raised QD-PCFSP sensor has attained the numerical amplitude and sensitivity of wavelength 230 RIU^{-1} and 15000 nm/RIU, respectively, which is an intensively larger value than the traditional PCF sensor and the wavelength sensitivity of 15,000 RIU^{-1} that admits the highest value in the literature. The larger wavelength sensitivity sensor will be very useful for remote biological, biomedical and biochemical analyte detection.

Conclusion

A Quasi D-shaped external Au metal-coated PCF inducing SPR sensor has been proposed and analyzed, which shows remarkable

Table 1
A comparison table with the existing sensor.

Ref.	Wavelength Range in (nm)	RI's Range	Wavelength Sensitivity in (nm/RIU)	Wavelength Resolution (RIU)	Amplitude Sensitivity in (RIU^{-1})	Corresponding Amplitude Resolution (RIU)
[31]	720–760	1.33–1.36	2000	5×10^{-5}	200	5×10^{-5}
[13]	550–650	1.33–1.37	5200	2.70×10^{-5}	216	4.62×10^{-5}
[18]	550–800	NA	7300	1.36×10^{-5}	216	4.62×10^{-5}
[33]	1000–1600	1.43–1.46	7700	1.29×10^{-5}	150	6.66×10^{-5}
[32]	550–1150	1.33–1.40	12,000	8.33×10^{-6}	1086	9.2×10^{-6}
[47]	–	1.4–1.46	16,000	6.25×10^{-6}	780	1.28×10^{-6}
Proposed Sensor	1080–1560	1.42–1.46	15,000	6.67 × 10–6	230	4.348×10^{-5}

amplitude sensitivity for the detection of different environmental samples. The sensing performances are optimized with varying sensor parameters like- gold film layer thickness and pitch parameter. The numerical results show the maximum amplitude and sensitivity of wavelength 560 RIU^{-1} and 15000 nm/RIU for sample measurement ranging from 1.42 RIU to 1.46 RIU. The corresponding maximum sensor resolution of the wavelength is 6.67×10^{-5} RIU and amplitude resolution is 4.348×10^{-5} RIU. Due to the use of gold as plasmonic material, the sensor can be practically implemented with moderate cost. Because of the low cost and extremely highly sensitive response, the proposed device can be potentially applied for various bio-samples such as biological, biomedical and biochemical analytes detection.

Authorship contribution statement

Md. Biplob Hossain: Conceptualization, Formal analysis, Investigation, Data curation, Writing - original draft, Writing - review & editing. **Md Shafayet Hossain:** Investigation, Data curation, Writing - original draft. **S.M. Riazul Islam:** Conceptualization, Formal analysis, Investigation, Data curation, Funding acquisition. **Md. Nazmus Sakib:** Conceptualization, Formal analysis, Investigation, Data curation, Writing - original draft, Writing - review & editing. **Khondoker Ziaul Islam:** Conceptualization, Formal analysis, Revision. **Md. Amzad Hossain:** Conceptualization, Formal analysis, Revision. **Md. Sanwar Hossain:** Conceptualization, Formal analysis, Revision. **A.S.M. Sanwar Hosen:** Formal analysis, Funding acquisition. **Gi Hwan Cho:** Formal analysis, Funding acquisition.

Declaration of Competing Interest

The authors declare that they have no known competing financial interests or personal relationships that could have appeared to influence the work reported in this paper.

Acknowledgement

This research was supported by the Sejong University through its Research Faculty Program (20192021).

References

[1] Rifat AA, Hasan MR, Ahmed R, Butt H. Photonic crystal fiber-based plasmonic biosensor with external sensing approach. J Nanophoton 2017.
[2] Hossain M, Rana M. DNA hybridization detection based on resonance frequency readout in graphene on Au SPR biosensor. J Sensors 2016;2016.
[3] Hossain MB, Akib TBA, Abdulrazak LF, Rana MM. Numerical modeling of graphene-coated fiber optic surface plasmon resonance biosensor for BRCA1 and BRCA2 genetic breast cancer detection. Opt Eng 2019;58(03):1. https://doi.org/10.1117/1.OE.58.3.037104.
[4] Nico J, Fischer MJ. Surface plasmon resonance: a general introduction. Surface Plasmon Resonance. Springer; 2010. p. 1–14.
[5] Hossain MB. Graphene-MoS2-Au-TiO2-SiO2 hybrid SPR biosensor for formalin detection: numerical analysis and development. Adv Mater Lett 2019;10.
[6] Hossain Md Biplob, Rana Md Masud, Abdulrazak Lway Faisal, Mitra Saikat, Rahman Mostafizur. Graphene-MoS2 with TiO2- SiO2layers based surface plasmon resonance biosensor: Numerical development for formalin detection. Biochem Biophys Rep 2019;18:100639.
[7] Khurgin JB, Boltasseva A. Reflecting upon the losses in plasmonics and metamaterials. MRS Bull 2012;37(8):768–79.
[8] Hossain MB, Rana MM, Abdulrazak LF, Mitra S, Rahman M. Design and analysis of graphene-MoS2 hybrid layer based SPR biosensor with TiO2-SiO2 nano film for formalin detection: numerical approach. Opt Quant Electron 2019;51(6):195–207.
[9] Hossain MB, Islam MM, Abdulrazak LF, Rana MM, Akib TBA, Hassan M. Graphene-coated optical fiber SPR biosensor for BRCA1 and BRCA2 breast cancer biomarker detection: a numerical design-based analysis. Photonic Sensors 2019;9(4):1–13.
[10] Wang F, Sun Z, Liu C, Sun T, Chu PK. A high-sensitivity photonic crystal fiber (PCF) based on the surface plasmon resonance (SPR) biosensor for detection of density alteration in non-physiological cells (DANCE). OptoElectron Rev 2018;26(1):50–6.
[11] Yuan Y, Ding L, Guo Z. Numerical investigation for SPR-based optical fiber sensor. Sens Actuators, B 2011;157(1):240–5.
[12] Filion-Côté S, et al. Design and analysis of a spectro-angular surface plasmon resonance biosensor operating in the visible spectrum. Rev Sci Instrum 2014;85(9):093107.
[13] N. Luan, R. Wang ,W. Lv, and J. Yao J, "Surface plasmon resonance sensor based on D-shaped microstructured optical fiber with hollow core."Optics Express, vol. 23, no. 7, pp. 8576, 2015.
[14] A. E. Khalil, A. H. EI-Saeed, M. A. Ibrahim, M. E. Hashish, M. R. Abdelmonem, M. Farhat, O. Hameed, M. Y. Azab, and S. S. A. Obayya, "Highly sensitive photonic crystal fiber biosensor based on titanium nitride," in Opt. Quant. Electron, vol. 50, no. 158, pp. 1-12, March 2018.
[15] M. Y. Azab, M. F. O. Hameed, A. Heikal, M. A. Swillam, and S. Obayya, "Analysis of highly sensitive surface plasmon photonic crystal fiber biosensor," Photonic Sensors 160, SPIE, 2018, 10541: 105411N-1-105411N-6.
[16] Razzak SMA, Namihira Y, Hossain MA, Khaleque A. Designing birefringence of index-guiding nonhexagonal photonic crystal fibers. J Opt 2011;40(2):56–64.
[17] Hasan MR, Akter S, Rahman MS, Ahmed K. Design of a surface plasmon resonance refractive index sensor with high sensitivity. Opt Eng 2017;56(8).
[18] Tian M, Lu P, Chen L, Ly C, Liu D. All-solid D-shaped photonic fiber sensor based on surface plasmon resonance. Opt Commun 2012;285(6):1550–4.
[19] Mahfuz MA, Mollah MA, Momota MR, Paul AK, Masud A, Akter S, et al. Highly sensitive photonic crystal fiber plasmonic sensor: design and analysis. Opt Mater 2019;90:315–21.
[20] Hasan MR, Akter S, Rifat AA, et al. Spiral photonic crystal fiber-based dual-polarized surface plasmon resonance biosensor. IEEE Sens J 2018;18(1):133–40.
[21] Kumar V, Singh S. Design of titanium nitride coated PCF-SPR sensor for liquid sensing applications. Optical Fiber Tech 2019;48:159–64.
[22] Paul AK, Sarkar AK, Rahman MABS, Khaleque A. Twin core photonic crystal fiber plasmonic refractive index sensor. IEEE Sens J 2018;18(14):5761–9.
[23] Alok Kumar PAUL, Sarkar Ajay Krishno, Khaleque Abdul. Dual-core photonic crystal fiber plasmonic refractive index sensor: A numerical analysis. Photon Sensors 2019;9(2):151–61.
[24] Hossain B, Tasnim T, Abdulrazak LF, Rana M, Islam R. A numerical approach to design the kretschmann configuration based refractive index graphene-MoS2 hybrid layers with TiO2-SiO2 nano for formalin detection. Photonic Sensors 2019;1–13. https://doi.org/10.1007/s13320-019-0566-5.
[25] Hossain MB, Rana MM. Graphene coated high sensitive surface plasmon resonance biosensor for sensing DNA hybridization. Sens Lett 2016;14:1–8.
[26] Gupta BD, Verma RK. Surface plasmon resonance-based fiber optic sensors: Principle, probe designs and some applications. J Sens 2009;2009(1):979761.
[27] Qin W, Li S, Yao Y, Xin X, Xue J. Analyte-filled core self-calibration microstructured optical fiber based plasmonic sensor for detecting high refractive index aqueous analyte. Opt Lasers Eng 2014;58:1–8.
[28] Shushama KN, Rana MM, Inum R, Hossain MB. Sensitivity enhancement of graphene coated surface plasmon resonance biosensor. Opt Quant Electron 2017;49(11):381.
[29] Tong K, Wang FC, Wang MT, Dang P, Wang YX, Sun JR. D-shaped photonic crystal fiber biosensor based on silver-graphene. Optik-Int J Light Electron Optics 2018;168:467–74.
[30] Fan Z, Li S, Liu Q, An G, Chen H, Li J, Chao D, Li H, Zi J, Tian W. High sensitivity of refractive index sensor based on analyte-filled photonic crystal fiber with surface plasmon resonance. IEEE Photon J 2015;7(3):3.
[31] S, Nivedha and Ramesh Babu, P and Senthilnathan, K. (2017). D-shaped plasmonic sensor using a molybdenum disulfide doped photonic crystal fiber. IOP Conference Series: Materials Science and Engineering. 263. 052031.
[32] Mohammad Al Mahfuz, Md. Aslam Mollah, Moriom Rojy Momota, Alok Kumar Paul, Al Masud, Sanjida Akter, Md. Rabiul Hasan,Highly sensitive photonic crystal

fiber plasmonic biosensor: Design and analysis,Optical Materials,Volume 90,2019, Pages 315-321,ISSN 0925-3467.
[33] Gangwar RK, Singh VK. Highly sensitive surface plasmon resonance based D-shaped photonic crystal fiber refractive index sensor. Springer Science + Business Media 2016.
[34] Ming Tian a, Ping Lu a,*, Li Chen a, Chao Lv a,b and Deming Liu a, All-solid D-shaped photonic fiber sensor based on surface plasmon resonance.
[35] Ze Zhang, Fenghong Chu, Zi Guo, Jinyu Fan, Gaofang Li and Wei Cheng, Design and Optimization of Surface Plasmon Resonance Sensor Based on Polymer-tipped Optical Fiber.
[36] Hossen MN, Ferdous M, Khalek MA, Chakma S, Paul BK, Ahmed K. Design and analysis of biosensor based on surface plasmon resonance. Sens Bio-Sens Res 2018;21:1–6.
[37] Luan N, Yao J. Refractive index and temperature sensing based on surface plasmon resonance and directional resonance coupling in a PCF. IEEE Photon J 2017;9(2):1–7.
[38] Monfared YE, Ponomarenko SA. Extremely nonlinear carbon-disulfide-filled photonic crystal fiber with controllable dispersion. Opt Mater 2019;88:406–11.
[39] Kabir MA, Hassan MM, Hossain MN, Paul BK, Ahmed K. Design and performance evaluation of photonic crystal fibers of supporting orbital angular momentum states in optical transmission. Opt Commun 2020;125731.
[40] Israk MF, Razzak MA, Ahmed K, Hassan MM, Kabir MA, Hossain MN, et al. Ring-based coil structure photonic crystal fiber for transmission of Orbital Angular Momentum with large bandwidth: Outline, investigation and analysis. Opt Commun 2020;126003.
[41] Mollah MA, Mazid MA, Ahmed K. Hi-bi photonic crystal fiber for broadband filter realization using copper microwires. Plasmonics 2020.
[42] Abdullah H, Mitu SA, Ahmed K. Magnetic fluid-injected ring-core-based micro-structured optical fiber for temperature sensing in broad wavelength spectrum. J Electron Mater 2020.
[43] Abdullah H, Ahmed K, Mitu SA. Ultrahigh sensitivity refractive index biosensor based on gold coated nano-film photonic crystal fiber. Results Phys 2020;103151.
[44] Paul BK, Ahmed K, El-Khozondar HJ, Pobre RF, Peña JSG, Merciales MC, et al. The design and analysis of a dual-diamond-ring PCF-based sensor. J Comput Electron 2020.
[45] Jiao S, Gu S, Yang H, Fang H, Xu S. Highly sensitive dual-core photonic crystal fiber based on a surface plasmon resonance sensor with a silver nano-continuous grating. Appl Opt 2018;57(28):8350–8.
[46] Ahmed T, Paul AK, Anower MS, Razzak SA. Surface plasmon resonance biosensor based on hexagonal lattice dual-core photonic crystal fiber. Appl Opt 2019;58(31):8416–22.
[47] Nazmus Sakib, Md, Riazul Islam SM, Mahendiran TV, Abdulrazak Lway Faisal, Islam Md Shofiqul, Mehedi Ibrahim Mustafa, et al. Numerical study of circularly slotted highly sensitive plasmonic biosensor: A novel approach. Results Phys 2020:103130.